WILEY-VCH

ARTICLE

Nanostar-shaped gold nanoparticles as friendly interfaces for protein electrochemistry – the case study of cytochrome *c*

Célia M. Silveira,[a] Rosaceleste Zumpano,[b] Miguel Moreira,[a] Miguel Peixoto de Almeida,[c] Maria João Oliveira,[a,d] Marina Bento,[a] Cláudia Montez,[a] Inês Paixão,[a] Ricardo Franco,[a] Eulália Pereira,[c] and M. Gabriela Almeida*[a,e]

To Professor Lo Gorton, for being a top researcher of his field and for his tremendous generosity and eternal youth.

Abstract: Gold nanostars with an average tip-to-tip length of 52 ± 6 nm were functionalized with different capping agents and used as electrode modification materials for protein electrochemistry. Direct electron transfer between cytochrome *c* and nanostars coated pyrolytic graphite electrodes was observed with the protein in solution. The electrochemical response was improved at nanostars functionalized with 1:1 mixture of 11-mercaptoundecanoic acid and 4-mercaptobezoic acid in comparison with gold nanospheres coated with a similar functionalization. Further immobilization of cytochrome *c* on pyrolytic graphite while conjugated with the same nanostars guaranteed the maintenance of the protein's native properties, whereas direct adsorption on the bare or nanostars modified electrodes resulted in an altered conformational state. The pseudo-peroxidase activity of the altered cytochrome *c* was enhanced in the presence of the nanostars.

Introduction

One of the main challenges for protein bioelectrochemistry is achieving efficient electronic coupling between the biomolecule and the electrode. This is particularly significant for direct electron transfer (DET) based systems, in which the protein exchanges electrons directly with the electrode. Very often the protein's redox centers are shielded by the polypeptide chain, imposing a kinetic barrier that prevents fast interfacial electron transfer (ET).[1] Important progress has been made by using nanostructured materials for electrode modification, such as metal nanoparticles.[2] Gold nanoparticles (AuNPs), in particular, provide not only a higher electrode area, but also a remarkable affinity for proteins, yielding a higher level of protein surface coverage while preserving biological activity.[3] In fact, many of the applications of AuNPs in bionanotechnology rely on the facile modification of the surface chemistry of AuNPs, providing a convenient scaffold for protein immobilization with excellent biocompatibility. In many cases, the different electrochemical behavior of proteins in AuNPs-modified electrodes cannot be explained solely by the increase in electroactive area and surface density. Other effects, such as favorable orientation of adsorbed proteins, changes of protein structure upon adsorption and catalytic activity of AuNPs, can also improve ET. This improved performance has been explored in numerous applications, particularly in the development of biosensors and enzymatic fuel cells.[4]

The use of AuNPs as electrode-modifiers has mainly focused on the optimization of the electrode responses, either by using different techniques to increase coverage/adhesion to the electrode surface or by using other nanomaterials (e.g. carbon based) to further increase performance. The advances so far are very promising, but the exact role of gold nanoparticles is still a matter of much debate. One of the reasons is that the interaction between proteins and AuNPs is a very complex process that depends on the properties of the AuNPs, namely size, shape and surface functionalization, in addition to the properties of the protein. For example, adsorption of proteins on AuNPs of different sizes can lead to different degrees of structural changes, due to the variation of curvature with size in spherical nanoparticles.[5] Shape can also influence adsorption[6] and reactivity,[7] because non-spherical nanoparticles expose high index crystal facets that have higher binding energies with the molecules adsorbed. Surface chemistry influences not only the extent of protein adsorption, but also the degree of protein denaturation upon adsorption. In addition, surface charge of the nanoparticle not only influences the electrostatic interaction with the protein, but also promotes adsorption through specific sites on the protein surface with opposite charge, leading to a preferred orientation of adsorbed proteins. Still, studies addressing these factors are scarce. The size of AuNPs has also been shown to influence the electrochemical behavior of adsorbed proteins. For instance, a

[a] Dr. C.M. Silveira, M. Moreira, M.J. Oliveira, M. Bento, C. Montez, I Paixão, Prof. Dr. R. Franco and Prof. Dr. M.G. Almeida
UCIBIO, REQUIMTE
Faculdade de Ciências e Tecnologia, Universidade NOVA de Lisboa
2829-516 Monte de Caparica, Portugal
E-mail: mg.almeida@fct.unl.pt
[b] R. Zumpano
Department of Chemistry and Drug Technologies
Sapienza University of Rome
Piazzale Aldo Moro 5, 00185 Rome, Italy
[c] Dr. M.P. Almeida and Prof. Dr. E. Pereira
LAQV, REQUIMTE, Dep. Química e Bioquímica
Faculdade de Ciências, Universidade do Porto
4169-007 Porto, Portugal
[d] M.J. Oliveira
i3N/CENIMAT, Dep. Ciência dos Materiais
Faculdade de Ciências e Tecnologia, Universidade NOVA de Lisboa and CEMOP/UNINOVA
2829-516 Caparica, Portugal
[e] Prof. Dr. M.G. Almeida
Centro de Investigação Interdisciplinar Egas Moniz (CiiEM)
Instituto Superior de Ciências da Saúde Egas Moniz
Campus Universitário, Quinta da Granja, 2829-511 Caparica, Portugal

Supporting information for this article is given via a link at the end of the document.

study of the electrochemical response of *Myrothecium verrucaria* bilirubin oxidase in sub-monolayers of AuNPs-modified electrodes showed an increase in maximum current with the growing size of the nanoparticles, which was entirely assigned to the increase of the surface area.[3c]

To our knowledge, non-spherical AuNPs have never been used to enhance protein DET. In particular gold nanostars (AuNSs), that have been widely used in optical biosensors based on their plasmonic properties, have been hardly used in modified electrodes, with a few examples in plasmon-enhanced electrochemistry[8] and in hydrogen peroxide[9] and heavy metal sensors.[10] Yet, gold nanostars have interesting properties that are worth to explore in bioelectrochemical applications, namely the presence of concave and convex surfaces in the same nanoparticle, providing protein adsorption sites with different properties; high surface areas compared with spherical or rod-shaped nanoparticles of similar size; and highly energetic crystal facets that can exhibit enhanced catalytic and adsorption properties.[11]

Herein, we employed gold nanostars as promoters of the DET reaction of cytochrome *c* (cyt *c*). The protein's electrochemical properties have been well studied,[12] as it is a prime model for understanding the mechanisms underlying protein ET and for the development of bioelectronic devices, such as amperometric biosensors.[1,13] The small, 13 kDa heme-containing protein, is primarily known as an electron shuttle in the mitochondrial ET chain; however cyt *c* plays other roles in biological processes, including in apoptosis and in the scavenging and production of reactive oxygen species.[13-14] Cyt *c* can adopt different conformational states that are thought to be of biological significance and a reflection of its multifunctional activities. The formation of alternative conformational species is induced by post-translational modifications, such as phosphorylation and methionine oxidations, or by the action of local electric fields (upon contact with ET partners, for example).[13-14] The interaction and adsorption of cyt *c* on some types of electrode can also generate the alternative states.[15] This has been exploited to gain a deeper insight into the dynamics of the ET reactions and redox-linked conformational changes of cyt *c*. For example, immobilization under high electric fields or hydrophobic interactions trigger conformational changes in cyt *c*, which include the dissociation of the methionine iron axial ligand and increased accessibility of potential substrates to the heme center. This can result in gain of peroxidase activity, a property that is frequently explored for the construction of hydrogen peroxide biosensors based on cyt *c*.[13]

In the present work, we have evaluated the DET reaction of cyt *c* at graphite electrodes modified with gold nanostars functionalized with different capping agents. The diffusion controlled electrochemistry of cyt *c* was investigated, as well as its behavior upon adsorption to the modified electrode or while electrostatically coupled to the gold nanostars, forming bionanoconjugates.

Results and Discussion

Characterization of gold nanostars

Gold nanostars (AuNSs) were synthesized in aqueous solution using the method of Yuan et. al.[16] TEM images (Figure S1) show that they have an average size of 52 ± 6 nm (tip-to tip) with 4-7 tips *per* particle. The nanoparticles were further characterized by DLS, measurement of zeta-potential and NTA. The average hydrodynamic diameter was 69.2 ± 3.4 and 62.4 ± 2.6 nm, by DLS and NTA, respectively, which is in agreement with the TEM results. In addition, NTA shows no significant aggregation of the AuNSs. Zeta-potential was -35.4 ± 3.1 mV, indicative of a good colloidal stability.

Electrochemical properties of gold nanostars modified electrodes

AuNSs functionalized with different capping agents, namely 11-mercaptoundecanoic acid (MUA), 1:1 mixture of MUA and 4-mercaptobenzoic acid (4-MBA), and the peptide CALNN (herein noted as AuNS@MUA; AuNS@MUA&4-MBA; AuNS@CALNN, respectively) were drop-casted on pyrolytic graphite (PG) electrodes and tested as electrochemical interfaces for ferricyanide, methyl viologen and cytochrome *c* (cf. experimental section configuration (a)). For comparison, spherical gold nanoparticles functionalized with MUA (AuNP@MUA) were also used, as well as, a control electrode without nanoparticles (bare PG).

a) Small redox mediators

To probe the performance of the AuNSs drop-casted on PG electrodes (AuNS/PG), we first carried out experiments with the $[Fe(CN)_6]^{3-}/[Fe(CN)_6]^{4-}$ redox couple, which typically displays quasi-reversible, surface sensitive electrochemical response. Analysis of the cyclic voltammograms (CVs) obtained in 1 mM $[Fe(CN)_6]^{3-}$ shows that the anodic and cathodic peak currents are identical and vary linearly with the square root of the scan rate, as expected for diffusion-controlled electrochemical processes (cf. Figure S2 for AuNS@MUA&4-MBA electrodes). The peak current intensities for all gold nanoparticle modified electrodes are in the same order of magnitude of the bare electrode (Figure 1a) and the peak separation increases (ΔEp > 100 mV, 50 mV s^{-1}) in comparison to the latter (ΔEp = 93 mV, Table 1). This means that the ET kinetics of the redox couple is slower at the gold nanoparticle films, a behavior that was attributed to the blocking effect of the capping agents, which are likely hindering interactions between the nanoparticles and the PG electrode.[17] The electrochemical reversibility decreases as follows: control > AuNP@MUA > AuNS@CALNN > AuNS@MUA&4-MBA > AuNS@MUA. These results show that the nature of the AuNSs capping agents influences the response of $[Fe(CN)_6]^{3-}$. In particular, unfavorable electrostatic interaction is expected between the anionic redox probe and the MUA and 4-MBA capping agents (cf. Figure S3), which are negatively charged at the working pH (7.0). Consequently, the electrochemical response is worse at these interfaces than at the CALNN peptide that confers a mostly polar hydrophilic character to the nanostars. Notably, the electrochemical performance of $[Fe(CN)_6]^{3-}$ at 15 nm spherical nanoparticles, functionalized with the worst performing AuNS capping agent, MUA (AuNP@MUA/PG), is improved in

comparison with the AuNS@MUA/PG electrode. This result indicates that the shape of the nanostructures is also important for the interaction with the redox probe. Possibly, the intrinsic properties of the nanoparticles, such as surface curvature, crystal facets exposed, etc. impact the electrochemical performance of the modified electrodes and explain the differences observed between AuNSs and AuNPs. Here, the flat gold surface in AuNPs is the one that most favors heterogeneous ET with $[Fe(CN)_6]^{3-}$.

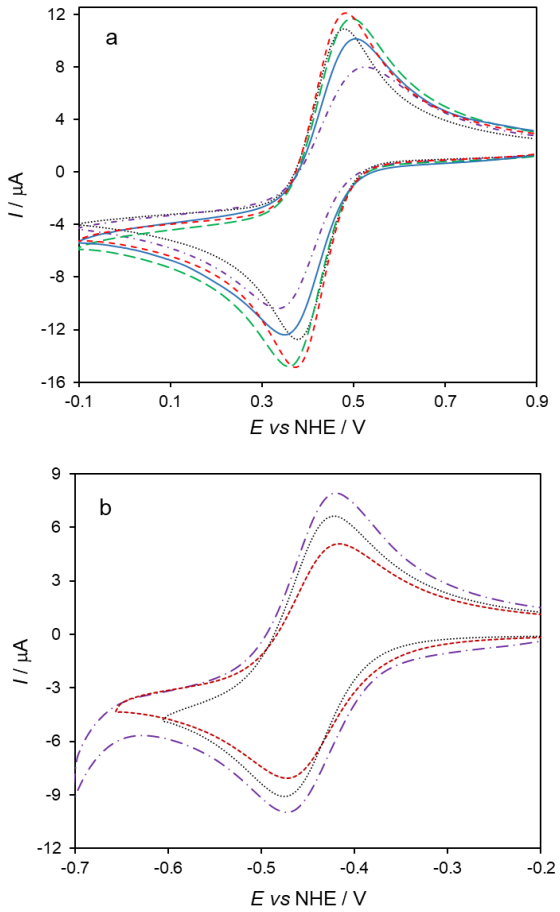

Figure 1. CVs of 1 mM a) ferricyanide and b) methyl viologen at bare PG (black dotted); AuNP@MUA (red short-dashed); AuNS@MUA (purple dash-dotted); AuNS@CALNN (green long-dashed) and AuNS@MUA&4-MBA (blue solid) modified PG electrodes. Measurements were done in 50 mM phosphate buffer, pH 7.0 at 50 mV s^{-1} scan rate.

In the next step, a positively charged redox probe, methyl viologen, was tested. Once again, the peak current intensities in all electrode configurations are in the same order of magnitude, but increasing as follows: AuNS@MUA > control > AuNP@MUA; experimental error, e.g. different PG electrodes surface areas or varying methyl viologen concentrations, can also account for the small variations observed. However, unlike the $[Fe(CN)_6]^{3-}$ assays, the ΔEp are identical for all tested interfaces (cf. Table 1). Thus, we conclude that the electrochemical reaction of methyl viologen is not greatly facilitated in comparison with the control electrode. Overall, these results show that a combination of charge and geometry of the nanostructures can affect the ET of small redox probes. In particular, the electric field enhancement at the stars tips[16] should directly influence the heterogeneous electrochemical reaction. Moreover, the intrinsic properties of the electronic mediators (e.g. structure rigidity of methyl viologen) could also account for the different interactions. At this stage, one cannot ascertain the contribution of each factor.

Table 1. Electrochemical characterization of ferricyanide and methyl viologen at the control and nanoparticle modified PG electrodes.

Redox probe	Ferricyanide		Methyl viologen	
Electrode modification	E°' *vs* NHE (V)	ΔEp (V)	E°' *vs* NHE (V)	ΔEp (V)
none	0.428	0.093	-0.449	0.047
AuNP@MUA	0.427	0.107	-0.444	0.051
AuNS@MUA	0.429	0.179	-0.445	0.048
AuNS@CALNN	0.426	0.132	-	-
AuNS@MUA&4-MBA	0.423	0.152	-	-

[a] Peak separations were determined at 50 mV s^{-1}.

No considerations about the estimation of the electroactive area of the modified electrodes could be done, because the electrochemical behavior of the redox probes strongly depends on the nanoparticles capping agent. Besides, the alternative method for the estimation of electroactive areas,[18] based on the calculation of gold surface oxides at the PG electrode in sulfuric acid, does not provide comparable results between the two gold morphologies. This is likely due to significantly different reactivities of nanospheres *vs* nanostars. In particular, the increased roughness of the AuNSs and the high index crystallinity of their tips, is expected to contribute to a higher reactivity for gold oxidation than the spherical nanoparticles,[19] as suggested by the substantial increase in cathodic peak currents observed at the voltammogram traced with the AuNS/PG electrodes (Figure S4). Though, given that the capacitive current is practically constant (cf. Figure 1), we assume that the surface area increase is not significant in the presence of the nanoparticles, as one would expect from a nanostructured electrode. In fact, the latter are known for providing large surface areas that are usefull for protein loading and interaction with analytes. These architectures are often obtained by multiple layer-by-layer depositions of the nanomaterials.[20] Herein, due to the single deposition procedure a sub-monolayer coverage is expected. In these conditions it may not be possible to take advantage of the large surface area-to-volume ratios of the nanostructured materials. Nevertheless, it is interesting to note that, based solely in geometric considerations, the total surface area of AuNPs added to the electrode is ca.

0.027 cm^2 (calculated based on the diameter estimated by UV-vis of 17.0 nm),[21] that would provide an increase of 40% of the electrode geometrical area (0.071 cm^2). For AuNSs, the total surface area is even higher, ca. 0.036 cm^2, (55% increase, estimated based on the method of de Puig et al.).[22] The apparent lack of increase in electroactive surface areas must then be related to some mechanism that is obstructing the available surface. This may include extensive aggregation of the nanoparticles at the electrode surface and/or unfavorable interaction between capping agents and redox probes.

b) Cytochrome c

We tested the AuNSs as promoters of protein DET by using cytochrome *c* (cyt *c*) as a model system and PG electrodes covered with a layer of nanostructured gold (AuNS/PG). As shown in Figure 2, the CVs display two current peaks that are ascribed to the one electron reduction and oxidation of cyt *c*'s heme iron (Fe^{3+}/Fe^{2+}). The two control electrodes are also presented for comparison (bare and AuNP@MUA/PG).

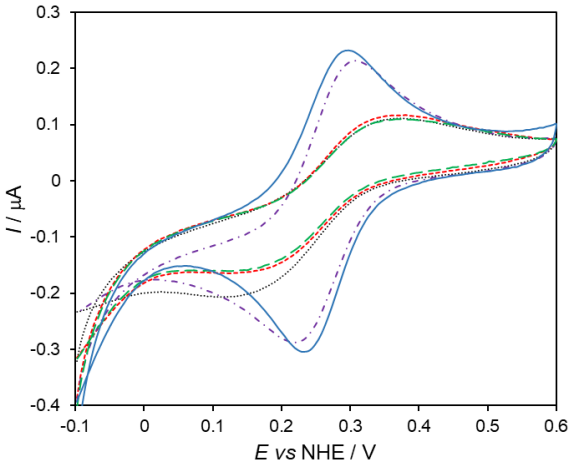

Figure 2. CVs of 0.2 mM cyt *c* at bare (black dotted); AuNP@MUA (red short-dashed); AuNS@MUA (purple dash-dotted); AuNS@CALNN (green long-dashed) and AuNS@MUA&4-MBA (blue solid) modified PG electrodes. Measurements were performed in 50 mM phosphate buffer, pH 7.0 at a scan rate of 5 mV s^{-1}.

Like $[Fe(CN)_6]^{3-}$ and methyl viologen, the electrochemical response of cyt *c* is a diffusion-controlled process, as the peak currents are proportional to the square root of the scan rate (not shown). The formal reduction potentials of cyt *c* at the different electrodes were determined from the midpoint peak potentials [(Epa + Epc)/2] of the CVs (Table 2). The $E^{0'}$ are constant over the whole scan rate range tested and in agreement with reported values for cyt *c* in solution.[12a,12c,23]

Table 2. Formal reduction potentials ($E^{0'}$) and peak separations (ΔEp at 5 mV s^{-1}) of cyt *c* at the control and nanoparticle modified electrodes.

Electrode modification	$E^{0'}$ *vs* NHE (V)	ΔEp (V)
none	0.252	0.266
AuNP@MUA	0.265	0.192
AuNS@MUA	0.273	0.125
AuNS@CALNN	0.275	0.245
AuNS@MUA&4-MBA	0.257	0.070

The peak current intensities are over two times higher for the AuNS@MUA and AuNS@MUA&4-MBA electrodes than for the control electrodes and AuNS@CALNN. Furthermore, the peak separations vary between 60 and 120 mV in the range of scan rates investigated, which is consistent with quasi-reversible electrochemical processes. In contrast, cyt *c* electrochemical response at the control (bare and AuNP@MUA) and AuNS@CALNN electrodes is very sluggish, as the ΔEp values are larger than 200 mV, even at the slowest scan rates (Table 2). These results indicate that the former surfaces, and in particular the AuNS@MUA&4-MBA interface, are better suited to promote the DET of cyt *c*. The capping agent should be playing a major role in the improved performance of these electrodes. In fact, the immobilization of cyt *c* on electrodes functionalized with carboxylic acid terminated alkanethiols, such as MUA and 4-MBA, is a commonly used strategy that has been extensively investigated.[23b,24] It is based on electrostatic interactions with the lysine residues that surround the partially exposed heme edge in cyt *c*, which constitute the site for electrostatic binding to physiological redox partners. Therefore, the cyt *c*'s heme group can be favorably oriented towards the electrode surface facilitating ET. Although we do not expect the protein to have adsorbed onto the AuNSs, as judged by its electrochemical behavior consistent with a diffusion based process, the heterogeneous ET reaction is clearly facilitated by the choice of anionic capping agents. Importantly, our results show that when using the same functionalization agent (MUA) the star-shaped nanostructures (AuNS@MUA) provide a more suitable microenvironment for DET with cyt *c* than the spherical nanoparticles (AuNP@MUA). This suggests that the shape of the nanostructures is an important factor for the interaction with redox proteins. Whether the impact of shape is due to the different facets exposed or to surface curvature effects is still not clear and further studies are necessary. As mentioned earlier, other properties of the nanoparticles, e.g. the strong electric field at the tips of the nanostars,[16] may also have a significant role in the ET reactions.

Immobilization of cytochrome *c* on gold nanostars modified electrodes

After selecting the 1:1 mixture of MUA and 4-MBA as the best performing capping agent (cf. Table 2), we evaluated cyt *c*'s DET reaction while the protein was immobilized on AuNS interfaces. Two types of electrodes were prepared: a layered system, consisting of a protein film deposited on AuNS/PG electrodes (cf. experimental section, configuration (c)) and cyt *c*–AuNS bionanoconjugates electrodes (configuration (b)). The bionanoconjugates were prepared by grafting the redox protein onto functionalized AuNSs. The decrease of the AuNSs' electrophoretic mobility on agarose gels confirmed the formation of the bionanoconjugates (Figure S5).[25] Samples with a cyt *c*/AuNS molar ratio of 200 were used for electrode preparation.

a) Cytochrome c-AuNS bionanoconjugates

The CVs obtained with AuNS@MUA&4-MBA@cyt *c* bionanoconjugates reveal a quasi-reversible redox couple with a formal reduction potential ($E^{0\prime}$) of 115 ± 9 mV (Figure 3a). This value is considerably less positive than the potential measured in solution for the same AuNSs (257 mV). However, similar shift trends have been reported for cyt *c* bound to negatively charged surfaces, including natural redox partners, like cytochrome *c* oxidase[26] or carboxylic acid terminated self-assembled monolayers (SAMs).[23b,24a] The lowering in potential is attributed to the neutralization of the cyt *c*'s surface charge upon adsorption to the negative surfaces.[23b,24a,27] The anodic and cathodic peak currents have a linear dependence on the scan rate in the range from 5 to 750 mV s^{-1} (Figure S6) and the peak-to-peak separation is only about 50 mV at the highest scan rate. This indicates that the immobilized cyt *c* has an almost ideal surface-controlled electrochemical behavior, and a potentially high ET rate constant (this parameter could not be estimated because the CVs measured above 750 mV s^{-1} did not display redox peaks).

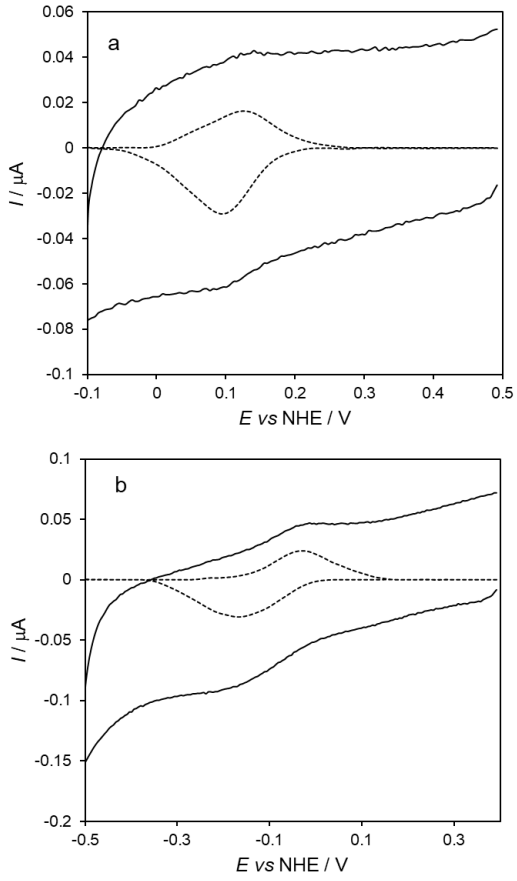

Figure 3. CVs of cyt *c* immobilized on PG electrodes a) bionanoconjugates (AuNS@MUA&4-MBA@cyt *c*/PG) and b) layer electrodes (cyt *c*/AuNS@MUA&4-MBA/PG). Experimental and baseline subtracted (x3) CVs are represented by the solid and dashed lines, respectively. Measurements were performed in 50 mM phosphate buffer, pH 7.0 at 50 mV s^{-1} scan rate.

b) Cytochrome c / AuNS layer electrodes

The direct electrochemical response of cyt *c* at the layer electrodes (cyt *c*/AuNS@MUA&4-MBA/PG, configuration (c)) is shown in Figure 3b. The protein's formal reduction potential is significantly lower in comparison with both the bionanoconjugates and solution potentials (-200 mV and -350 mV, respectively). The same is observed in the control assay with bare pyrolytic graphite (cyt *c*/PG, Figure S7). The large downshift in the reduction potential is consistent with the presence of non-native conformations of the protein at the electrode surface, as previously reported for cyt *c* adsorbed on different types of electrodes, including PG.[13,15,24a] This is not surprising, given the low AuNSs coverage obtained by the single deposition method used to prepare the electrodes (cf. discussion above). Consequently, cyt *c* is most likely distributed between the deposited AuNSs and non-coated PG surface. Accordingly, the PG electrode should be the main contributor for the formation of non-native cyt *c* species. The negative shift in redox potential of cyt *c*'s alternative conformational states has been attributed to changes in the heme environment and ligation state. Specifically,

the methionine axial iron ligand is dissociated in all identified non-native cyt *c* species; the coordination site may be left vacant or be occupied by a histidine residue or a water molecule.[13,15c] Since these altered conformations display peroxidase activity, in the next step, the electrodes with immobilized cyt *c* were placed in a solution containing 20 µM hydrogen peroxide (Figure 4).

c) Assessing the peroxidase activity of immobilized cytochrome c

The CVs recorded at the cyt *c*/AuNS@MUA&4-MBA/PG electrodes reveal increased cathodic peak current, at ca. -200 mV. This indicates that the cyt *c* immobilized in the layer electrode is able to catalyze hydrogen peroxide reduction; the molecule binds to the heme center and its subsequent reduction to water can be achieved with electrons delivered by the electrode.

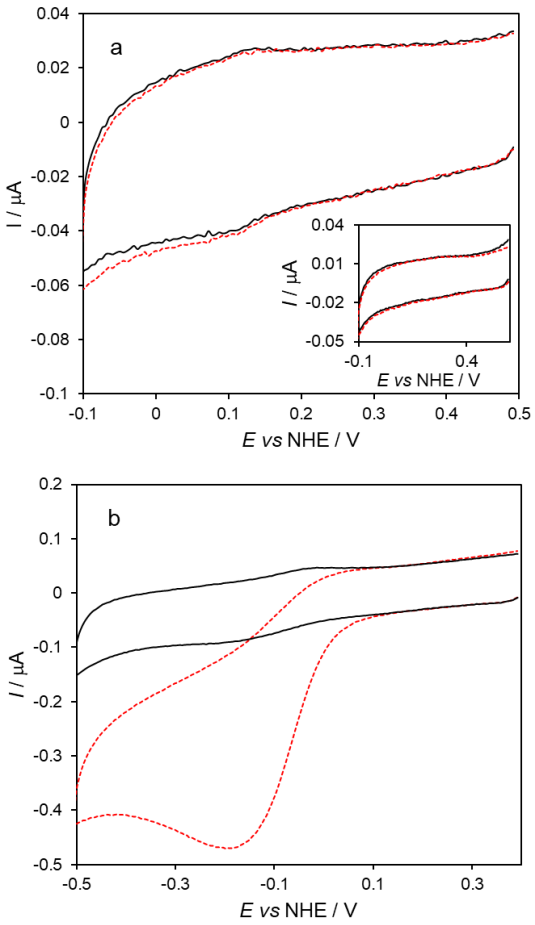

Figure 4. CVs of cyt *c* immobilized on PG electrodes in the absence (black solid) and presence (red dashed) of hydrogen peroxide (20 µM). a) Bionanoconjugate electrode (AuNS@MUA&4-MBA@cyt *c*/PG), inset: control electrode without cyt *c* (AuNS@MUA&4-MBA/PG). b) layer electrode (cyt *c*/AuNS@MUA&4-MBA/PG). Measurements were performed in 50 mM phosphate buffer, pH 7.0 at 50 mV s^{-1} scan rate.

In contrast, the bionanoconjugate electrodes show only a residual increase of cathodic current, most likely due to hydrogen peroxide direct reduction on the electrode, as observed in the control assay, i.e. absence of cyt *c* (Figure 4a, inset). Taken together, these results confirm that cyt c maintains its native conformation when linked to the AuNSs in the form of bionanoconjugates, but not when directly deposited on the AuNSs surface (layer electrodes). The pseudo-peroxidase activity of the cyt *c*/AuNS@MUA&4-MBA/PG electrodes was further investigated to determine the potential application in hydrogen peroxide biosensing. The cathodic currents progressively increase and the peak potentials shift to more negative values with increasing hydrogen peroxide in the cell, indicating a typical electrocatalytic behavior (Figure 5a). The catalytic current increases as a function of hydrogen peroxide concentration and eventually reaches a limiting value above 100 µM, which is consistent with a Michaelis-Menten type enzyme saturation kinetics (Figure 5b). The response of the bioelectrode is linear from 1.0 to 20 µM, with a detection limit of 0.49 µM at a signal to noise ratio of 3 (Figure 5b, inset). The sensitivity to hydrogen peroxide, determined from the slope of the calibration plot within the linear range, is 281 ± 21 $mA.M^{-1}.cm^{-2}$. We have compared the catalytic performance of the cyt c/AuNS bioelectrode with the control electrode without AuNSs, i.e., cyt *c*/PG. The current response varies linearly with hydrogen peroxide in the same range of concentrations than the cyt c/AuNS electrode (Figure S7), but with lower sensitivity (174 ± 8 $mA.M^{-1}.cm^{-2}$). This result confirms that the PG surface triggers the peroxidase activity of cyt *c* (due to the formation of non-native states of the protein). On the other hand, the increased sensitivity obtained in the presence of the AuNSs shows that the nanostructures can function as effective ET relays for cyt *c*, thereby facilitating the catalytic reaction.

Conclusions

In this work, functionalized gold nanostars are used as interfaces to promote the electrochemical response of cyt *c*. To the best of our knowledge this is the first use of AuNSs for the improvement of protein DET. Cyt *c*'s ET reaction is favored by the AuNSs interfaces in comparison with AuNPs based electrodes, thus demonstrating that the shape of the nanoparticle is an important property in what concerns their role as facilitators of protein DET. Further studies are necessary to assess the reasons for this enhanced behavior.

The AuNSs are also shown to provide a favorable microenvironment for the immobilization of cyt *c*, as conjugation with the AuNSs and subsequent adsorption on the PG electrode enables preserving the protein's native properties. In contrast, an altered conformational state of cyt *c* is induced by direct adsorption onto AuNSs modified and bare PG electrodes. Interestingly, this alternative conformation displays enhanced pseudo-peroxidase activity in the presence of the nanostars. The strategy shows promise for the construction of electrochemical biosensors based on protein DET.

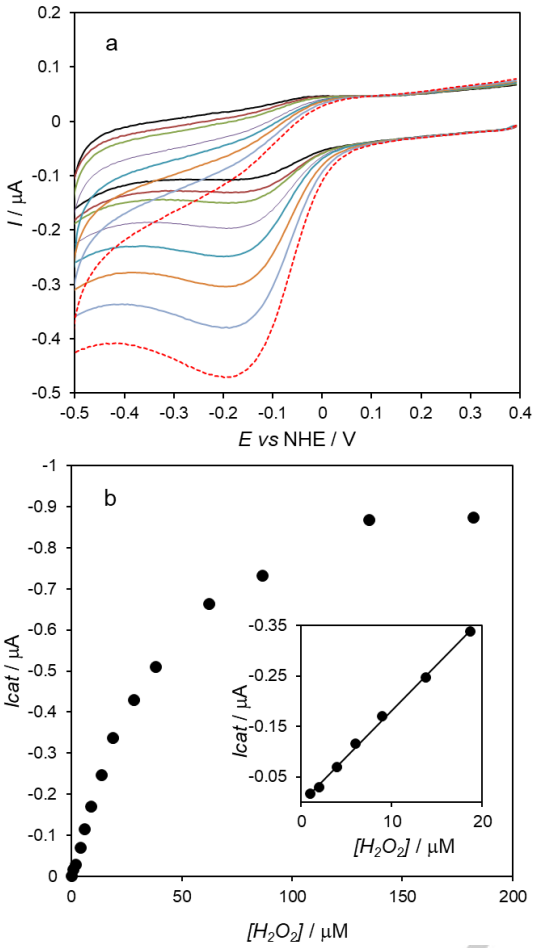

Figure 5. a) Electrochemical response of cyt *c*/AuNS@MUA&4-MBA/PG to varying hydrogen peroxide concentrations (0 – 20 µM, from black to red) in 50 mM phosphate buffer, pH 7.0 purged with argon. Scan rate 50 mV s^{-1}. b) Response of the bioelectrode to hydrogen peroxide additions. Inset: linear response range.

Experimental Section

Reagents

All reagents were obtained from Sigma-Aldrich, except CALNN and hydrogen peroxide solution 30 % (v/v) that were from CASLO Laboratory and Merck, respectively. Reagents were used as received.

Horse heart cytochrome *c* (cyt *c*) solutions were prepared in 50 mM phosphate buffer, pH 7.0; concentrations were determined spectrophotometrically using a molar absorptivity of 29.5 mM^{-1} cm^{-1} at 551 nm (for the reduced form), as instructed by the supplier. Similarly, the concentration of hydrogen peroxide stock solutions was determined using a molar absorptivity of 43.6 M^{-1} cm^{-1} at 240 nm; solutions were prepared immediately before use.

Solutions were prepared with deionized water (> 18.2 MΩ cm) obtained from a Millipore MilliQ water purification system. Glassware used during the synthesis and functionalization of gold nanoparticles was washed with *aqua regia* and then thoroughly rinsed with water, before use.

Synthesis and functionalization of nanoparticles

Spherical gold nanoparticles (AuNPs, 17 nm) were prepared using an extended Turkevich–Frens method, as described elsewhere.[28] Briefly, 2 mL of 0.34 M citrate solution was added to 98 mL of boiling ultrapure water, under stirring. After 5 minutes, 69 µL of 1.445 M $HAuCl_4$ solution was added. After 5 minutes, the solution turned from light yellow to dark red, and then it was left at room temperature. The suspension was then filtered (cellulose acetate 0.2 µm syringe filter) and stored at 4 ºC.

Gold nanostars (AuNSs) were synthesized using the method described by Yuan et al.[16] 1.76 mL of AuNPs suspension (8.5 nM), prepared as described above, were added as seeds to 87 mL of water with stirring, followed immediately by 24 µL of 1.445 M $HAuCl_4$ solution. Then, 703 µL of 100 mM ascorbic acid solution and 703 µL of 4 mM silver nitrate solution were added simultaneously. The suspension turned immediately to dark blue. The resulting AuNSs were washed by centrifugation at 2600 *g* for 30 minutes, and re-dispersed in water.

The nanoparticles were functionalized with bifunctional alkanethiols. A 10 mM ethanolic solution of the thiols (11-mercaptoundecanoic acid (MUA), 1:1 mixture of 11-mercaptoundecanoic acid and 4-mercaptobenzoic acid (MUA&4-MBA), and CALNN) was added to the NPs suspension under vigorous stirring. The solution was allowed to react overnight at 4 ºC to ensure a complete exchange of the original capping agent (citrate/ascorbate) by the desired bifunctional alkanethiol; excess of capping agent was removed by centrifugation at 2500 *g* for 10 min at 10 ºC, followed by re-dispersion in phosphate buffer (5 mM, pH 7.0). A red-shift of the LSPR peak observed by UV-Vis spectroscopy confirmed a successful functionalization. Possible aggregation was always checked by a UV-Vis before use. Nanoparticle suspensions were washed twice by centrifugation with basified water (pH 8) and sonicated.

Characterization of gold nanostars

Gold nanostars were characterized by UV-Vis spectroscopy, dynamic light scattering (DLS), electrophoretic light scattering (ELS), nanoparticle tracking analysis (NTA) and transmission electron microscopy (TEM). UV-Vis was performed in a Varian Cary 50 Bio spectrophotometer using quartz cells. DLS and ELS were performed using a Malvern Zetasizer NanoZS. The results are an average of three measurements for the same sample, performed at 25 ºC, with light detection at 273º (DLS) and at 17º using the backscatter mode (ELS). NTA was performed in a Malvern Nanosight NS300 (equipped with a 642 nm laser module); NTA results were obtained after the tracking analysis of 5 videos of 1 minute each, captured in 5 different parts of the sample (still mode). The results were then merged in a single size distribution. TEM was performed using a Hitachi H8100 microscope (Microlab, Instituto Superior Técnico, Lisboa, Portugal).

Bionanoconjugates preparation

Cyt *c*-AuNS bionanoconjugates were produced by adding cyt *c* (final concentration 0.2 µM) to aliquots of functionalized NPs (at 1 nM, determined by NTA) followed by overnight incubation at 4 ºC. These samples were then centrifuged at 2500 *g* for 2.5 min (10 ºC) and the colorless supernatant was removed and discarded. The pellet was re-dispersed in phosphate buffer (5 mM, pH 7.0) at the same volume (AuNSs at 1 nM) and kept at 4 ºC until use (within one week). Agarose gel electrophoresis, used to confirm conjugation, was performed as described elsewhere.[25] Briefly, a 0.3% (w/v) agarose gel was loaded with 15 µL of bionanoconjugate samples prepared at different cyt *c*/AuNS molar ratios (0 to 200). Electrophoresis was done in TAE buffer (1/8 X) in a mini-sub cell GT horizontal system (Bio-Rad), running for 20 min at 150 V and at room temperature. Results were processed by the eReuss software to analyze individual band migration. eReuss is a free and open source electrophoresis gel image processing software, available for download at https://github.com/lkrippahl/eReuss.

Electrode preparation

Before each experiment, the working pyrolytic graphite (PG) electrode was thoroughly polished with 0.3 μm alumina suspension (Buehler), rinsed and sonicated in deionized water for 5 min. The electrode was then dried with compressed air. Modifications were done by drop casting 5 μL of AuNSs (1 nM), bionanoconjugates (1 nM) or cyt *c* solution (0.2 mM) onto the surface of the working electrode. Each layer was allowed to dry at room temperature (ca. 20 min) before a new layer was applied. The PG electrodes were covered as follows: a) nanoparticles (AuNS/PG), b) bionanoconjugates (bioconj/PG) and c) protein over nanoparticles layer (cyt *c*/AuNS/PG) electrodes. Electrodes and solutions were stored at 4 ºC when not in use.

Electrochemical measurements

An EcoChemie potentiostat, Model Autolab 12, controlled with GPES 4.9 software (Metrohm) was used for all cyclic voltammetry measurements. An Ag/AgCl (saturated KCl) reference electrode (Radiometer), a platinum plate counter electrode (Radiometer) and a pyrolytic graphite working electrode (basal plane, Ø = 3 mm, made in-house with graphite from GE Healthcare) were used in a conventional three-electrode cell configuration. All experiments were performed at room temperature in 50 mM phosphate buffer, pH 7.0, as supporting electrolyte. The electrochemical cell, containing 10 mL of supporting electrolyte, was thoroughly purged with argon before starting the experiments (20 min). Cyclic voltammograms (CVs) were acquired in a 5 - 1000 mV s^{-1} scan rate range. Ferricyanide and methyl viologen were assayed in solution (1 mM) using configuration (a) only (cf. previous section); while cyt *c* was studied using configurations (a), (b) and (c). Response of the bioconj/PG (b) and cyt *c*/AuNS/PG (c) electrodes to hydrogen peroxide was evaluated upon successive additions of small volumes of freshly prepared stock solutions to the electrochemical cell. After each addition, the electrolyte was purged with argon to remove dissolved dioxygen and a new CV was recorded (experiments performed at 50 mV s^{-1}). Catalytic currents were determined at –0.45 V and corrected by subtracting the background current measured in the absence of hydrogen peroxide. All potentials are quoted versus the NHE reference electrode (+0.197 V *vs* Ag/AgCl).

Acknowledgements

The authors are grateful to Fundação para a Ciência e a Tecnologia (MCTES funds) and European Union (European Social Fund and European Regional Development Fund), for financial support through grants UID/QUI/50006/2019 and POCI-01-0145-FEDER-007265 (LAQV-REQUIMTE), UID/Multi/04378/2019 and POCI-01-0145-FEDER-007728 (UCIBIO-REQUIMTE), PTDC/NAN-MAT/30589/2017, all from COMPETE and COMPETE 2020 programs, grant NORTE-01-0145-FEDER-000011, from NORTE 2020 program, and fellowships SFRH/BD/95983/2013 (to M.P.A.), from POCH program, and SFRH/BD/132057/2017 (to M.J.O.), from the MIT-Bioengineering PhD Program. REQUIMTE is acknowledged by a Porto-Caparica collaborative Grant “NanoBE – Innovative Gold Nanostructured Interfaces for Electrochemical Biosensing”. All programs from QREN (COMPETE) or Portugal 2020 (all others) partnership agreements.

Keywords: Gold nanostars • Nanoparticles • Protein electrochemistry • Cytochrome *c* • Direct electron transfer

[1] T. Nöll, G. Nöll, *Chem. Soc. Rev.* **2011**, *40*, 3564-3576.

[2] a) M.-C. Daniel, D. Astruc, *Chem. Rev.* **2004**, *104*, 293-346; b) W. Putzbach, N. J. Ronkainen, *Sensors* **2013**, *13*, 4811-4840; c) C. Zhu, G. Yang, H. Li, D. Du, Y. Lin, *Anal. Chem.* **2015**, *87*, 230-249.

[3] a) M. Kizling, M. Dzwonek, A. Wieckowska, R. Bilewicz, *Curr. Opin. Electrochem.* **2018**, *12*, 113-120; b) M. Kizling, M. Dzwonek, A. Więckowska, R. Bilewicz, *ChemCatChem* **2018**, *10*, 1988-1992; c) D. Pankratov, R. Sundberg, D. B. Suyatin, J. Sotres, A. Barrantes, T. Ruzgas, I. Maximov, L. Montelius, S. Shleev, *RSC Adv.* **2014**, *4*, 38164-38168.

[4] J. M. Pingarrón, P. Yáñez-Sedeño, A. González-Cortés, *Electrochim. Acta* **2008**, *53*, 5848-5866.

[5] a) A. Arsalan, H. Younus, *Int. J. Biol. Macromol.* **2018**, *118*, 1833-1847; b) S. Tadepalli, Z. Wang, J. Slocik, R. R. Naik, S. Singamaneni, *Nanoscale* **2017**, *9*, 15666-15672.

[6] R. García-Álvarez, M. Hadjidemetriou, A. Sánchez-Iglesias, L. M. Liz-Marzán, K. Kostarelos, *Nanoscale* **2018**, *10*, 1256-1264.

[7] a) D. D. Robertson, M. L. Personick, *Chem. Mater.* **2019**, *31*, 1121-1141; b) B.-H. Wu, J.-Y. Chung, L.-Y. Hung, M.-C. Cheng, S.-M. Peng, I. C. Chen, *ACS Omega* **2019**, *4*, 5327-5334.

[8] a) C. Wang, X.-P. Zhao, Q.-Y. Xu, X.-G. Nie, M. R. Younis, W.-Y. Liu, X.-H. Xia, *ACS Appl. Nano Mater.* **2018**, *1*, 5805-5811; b) S.-S. Wang, W.-C. Hu, F.-F. Liu, Q.-Y. Xu, C. Wang, *Electrochim. Acta* **2019**, *301*, 359-365.

[9] Y. Li, J. Ma, Z. Ma, *Electrochim. Acta* **2013**, *108*, 435-440.

[10] S. Dutta, G. Strack, P. Kurup, *Sens. Actuators, B* **2019**, *281*, 383-391.

[11] A. Guerrero-Martínez, S. Barbosa, I. Pastoriza-Santos, L. M. Liz-Marzán, *Curr. Opin. Colloid Interface Sci.* **2011**, *16*, 118-127.

[12] a) P. Yeh, T. Kuwana, *Chem. Lett.* **1977**, *6*, 1145-1148; b) M. J. Eddowes, H. A. O. Hill, *J. Chem. Soc., Chem. Commun*. **1977**, 771b-772; c) W. Jin, U. Wollenberger, F. F. Bier, A. Makower, F. W. Scheller, *Bioelectrochem. Bioenerg.* **1996**, *39*, 221-225.

[13] D. Alvarez-Paggi, L. Hannibal, M. A. Castro, S. Oviedo-Rouco, V. Demicheli, V. Tórtora, F. Tomasina, R. Radi, D. H. Murgida, *Chem. Rev.* **2017**, *117*, 13382-13460.

[14] M. Hüttemann, P. Pecina, M. Rainbolt, T. H. Sanderson, V. E. Kagan, L. Samavati, J. W. Doan, I. Lee, *Mitochondrion* **2011**, *11*, 369-381.

[15] a) P. M. De Biase, D. A. Paggi, F. Doctorovich, P. Hildebrandt, D. A. Estrin, D. H. Murgida, M. A. Marti, *J. Am. Chem. Soc.* **2009**, *131*, 16248-16256; b) P. M. Paes de Sousa, S. R. Pauleta, M. L. Simões Gonçalves, G. W. Pettigrew, I. Moura, J. J. Moura, M. M. Correia dos Santos, *J. Biol. Inorg. Chem.* **2011**, *16*, 209-215; c) H. Wackerbarth, P. Hildebrandt, *ChemPhysChem* **2003**, *4*, 714-724.

[16] H. Yuan, C. G. Khoury, H. Hwang, C. M. Wilson, G. A. Grant, T. Vo-Dinh, *Nanotechnol.* **2012**, *23*, 075102-075102.

[17] R. A. Clark, C. J. Trout, L. E. Ritchey, A. N. Marciniak, M. Weinzierl, C. N. Schirra, D. Christopher Kurtz, *J. Electroanal. Chem.* **2013**, *689*, 284-290.

[18] S. Trasatti, O. A. Petrii, *J. Electroanal. Chem.* **1992**, *327*, 353-376.

[19] a) M. Mavrikakis, P. Stoltze, J. K. Nørskov, *Catal. Lett.* **2000**, *64*, 101-106; b) D. Su, S. Dou, G. Wang, *NPG Asia Mater.* **2015**, *7*, e155.

[20] a) N. Baig, M. Sajid, T. A. Saleh, *TrAC, Trends Anal. Chem.* **2019**, *111*, 47-61; b) I. Taurino, G. Sanzò, R. Antiochia, C. Tortolini, F. Mazzei, G. Favero, G. De Micheli, S. Carrara, *TrAC, Trends Anal. Chem.* **2016**, *79*, 151-159.

[21] W. Haiss, N. T. K. Thanh, J. Aveyard, D. G. Fernig, *Anal. Chem.* **2007**, *79*, 4215-4221.

[22] H. de Puig, J. O. Tam, C.-W. Yen, L. Gehrke, K. Hamad-Schifferli, *J. Phys. Chem. C* **2015**, *119*, 17408-17415.

[23] a) S. A. Mozaffari, T. Chang, S.-M. Park, *J. Phys. Chem. C* **2009**, *113*, 12434-12442; b) J. Petrović, R. A. Clark, H. Yue, D. H. Waldeck, E. F. Bowden, *Langmuir* **2005**, *21*, 6308-6316.

[24] a) X. Chen, R. Ferrigno, J. Yang, G. M. Whitesides, *Langmuir* **2002**, *18*, 7009-7015; b) M. Fedurco, *Coord. Chem. Rev.* **2000**, *209*, 263-331.

[25] M. P. Almeida, P. Quaresma, S. Sousa, C. Couto, I. Gomes, L. Krippahl, R. Franco, E. Pereira, *Phys. Chem. Chem. Phys.* **2018**, *20*, 16761-16769.

[26] A. S. Haas, D. L. Pilloud, K. S. Reddy, G. T. Babcock, C. C. Moser, J. K. Blasie, P. L. Dutton, *J. Phys. Chem. B* **2001**, *105*, 11351-11362.

[27] T. M. Yawitz, K. S. Patterson, B. X. Onkst, F. Youmbi, R. A. Clark, *J. Electroanal. Chem.* **2018**, *828*, 59-62.

[28] K. Zabetakis, W. E. Ghann, S. Kumar, M.-C. Daniel, *Gold Bull.* **2012**, *45*, 203-211.

Entry for the Table of Contents

ARTICLE

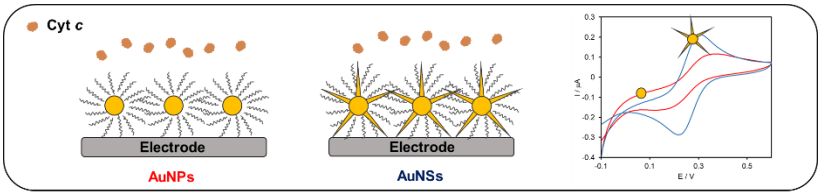

*C.M. Silveira, R. Zumpano, M. Moreira, M.P. Almeida, M.J. Oliveira, M. Bento, C. Montez, I. Paixão, R. Franco, E. Pereira and M.G. Almeida**

Page No. – Page No.
Nanostar-shaped gold nanoparticles as friendly interfaces for protein electrochemistry – the case study of cytochrome c